How to cite: *Angew. Chem. Int. Ed.* **2022,** *61,* e202203646
International Edition: doi.org/10.1002/anie.202203646
German Edition: doi.org/10.1002/ange.202203646

Aluminium Ion Batteries | Hot Paper

Heterocyclic Conjugated Polymer Nanoarchitectonics with Synergistic Redox-Active Sites for High-Performance Aluminium Organic Batteries

Xiyue Peng[+], Yuan Xie[+], Ardeshir Baktash, Jiayong Tang, Tongen Lin, Xia Huang, Yuxiang Hu, Zhongfan Jia, Debra J. Searles, Yusuke Yamauchi, Lianzhou Wang,* and Bin Luo**

Abstract: The development of cost-effective and long-life rechargeable aluminium ion batteries (AIBs) shows promising prospects for sustainable energy storage applications. Here, we report a heteroatom π-conjugated polymer featuring synergistic C=O and C=N active centres as a new cathode material in AIBs using a low-cost $AlCl_3$/urea electrolyte. Density functional theory (DFT) calculations reveal the fused C=N sites in the polymer not only benefit good π-conjugation but also enhance the redox reactivity of C=O sites, which enables the polymer to accommodate four $AlCl_2(urea)_2^+$ per repeating unit. By integrating the polymer with carbon nanotubes, the hybrid cathode exhibits a high discharge capacity and a long cycle life (295 mAh g^{-1} at 0.1 A g^{-1} and 85 mAh g^{-1} at 1 A g^{-1} over 4000 cycles). The achieved specific energy density of 413 Wh kg^{-1} outperforms most Al–organic batteries reported to date. The synergistic redox-active sites strategy sheds light on the rational design of organic electrode materials.

Introduction

The development of efficient energy storage systems is of urgent need in modern society, motivated by the expansion of renewable energy and the growing demand for electric vehicles and mobile devices.[1] Combined with safety and sustainability concerns, current research interest has shifted towards safer and more earth-abundant materials in order to replace lithium ion battery systems.[2,3] Aluminium ion batteries (AIBs) have emerged as one of the most promising alternative energy storage technologies because of their high volumetric capacity (8040 mAh cm^{-3} for Al vs. 2046 mAh cm^{-3} for Li) and abundant aluminium reserves for large-scale electrical energy storage. Many types of inorganic cathode materials have been developed so far, including carbon materials,[4,5] metal dichalcogenides[6–8] and phosphides.[9,10] Carbon materials are prone to deliver high operating voltage and long cycling life, however, show limited capacities due to the sluggish intercalation/de-intercalation processes of large-sized $AlCl_4^-$ anions.[11] Regarding transition metal-chalcogen compounds, although they are reported with higher capacities than carbons, the materials suffer from capacity fading caused by irreversible phase transfer and even destruction of the original lattice during Al^{3+} intercalation.[12] Therefore, the lack of suitable cathode materials with high capacity, good cycling stability and reversible transport of aluminium carrier ions (i.e. $AlCl_4^-$, $AlCl_2^+$ or $AlCl_2(urea)_2^+$) have been the most imminent challenges that hinder AIBs from practical applications.

Organic redox-active materials are poised to become a competitive option to design low-cost, sustainable, and high-

[*] X. Peng,[+] Dr. Y. Xie,[+] Dr. A. Baktash, J. Tang, T. Lin, Dr. X. Huang, Prof. D. J. Searles, Prof. Y. Yamauchi, Prof. L. Wang, Dr. B. Luo
Australian Institute for Bioengineering and Nanotechnology,
The University of Queensland
St. Lucia, QLD, 4072 (Australia)
E-mail: y.yamauchi@uq.edu.au
l.wang@uq.edu.au
b.luo1@uq.edu.au

Dr. A. Baktash, J. Tang, T. Lin, Dr. X. Huang, Prof. Y. Yamauchi, Prof. L. Wang
School of Chemical Engineering,
The University of Queensland
St. Lucia, QLD, 4072 (Australia)

Prof. D. J. Searles
School of Chemistry and Molecular Biosciences,
The University of Queensland
St, Lucia, QLD, 4072 (Australia)

Prof. Y. Hu
Key Laboratory of Advanced Functional Materials of Education Ministry of China, Faculty of Engineering and Manufacturing,
Beijing University of Technology
Beijing, 100124 (China)

Dr. Z. Jia
Institute for Nanoscale Science and Technology,
College of Science and Engineering, Flinders University
Bedford Park, South Australia 5042 (Australia)

[+] These authors contributed equally to this work.

performance rechargeable batteries.[13–15] Compared with inorganic electrode materials from transition metal resources, organic electrodes constituted by light, inexpensive and sustainable elements such as C, H, O, N and S can satisfy the need with lower environmental footprints and greater safety in production and disposal.[16] In addition, the structural flexibility and weak intermolecular interactions in organic materials allow reversible diffusion and storage of bulky aluminium carrier ions, free from severe structural change issues as most inorganic ones suffer.[17] Furthermore, the organic electrodes normally undergo an "ion coordination" storage mechanism, which is in sharp contrast with the sluggish kinetics of certain inorganic compounds due to their strong coulombic interactions with aluminium carrier ions.[18]

Encouragingly, recent years have witnessed the bloom of a vast array of organic materials consisting of versatile redox-active functional groups, such as carbonyl group (C=O),[19,20] pyrazine/imine group (C=N),[21–23] and cyano group (C≡N)[24] as working centres. Among them, quinones stand out for their high theoretical capacity, high redox potential, and multi-electron reaction. Regardless of para or ortho quinone, the electron reduction of the contiguous carbonyl groups will take place, leading to the formation of negative enolates to chelate with aluminium carrier ions to stabilize the form.[19,25] Recent research on quinones intend to increase the carbonyl groups in one structure.[20,26] Nevertheless, it is found that the two or three neighbouring carbonyl groups can only chelate with one bulky aluminium carrier ion, which no doubt limits the effective utilization of the active sites and hampers the potential capacities.[27] Notably, nitrogen-containing heteroaromatic compounds can also be involved in reversible redox reactions with aluminium carrier ions, unfortunately they present relatively low operating potential and unimpressive battery performances.[21,22] Despite these efforts, there have been no reports in designing organic cathode materials with synergistically multiple active centres for AIBs and investigate the associated redox reactions. In this context, heterocycle-conjugate polymer nanoarchitectonics that involve molecular manipulation of organic molecules with redox-active C=O and C=N centres together with π-conjugation in one structure could provide new platform to develop advanced electrode materials for aluminium–organic batteries with high capacity, long cyclability, and high energy/power density.[28–30]

Herein, we present a nitrogen-containing heterocyclic quinone polymer named poly(4,5-dihydrophenanthro[4,5-*abc*]pyrazino [2,3-i]phenazine-10,15-dione), for the first time, as a high-performance organic cathode material in rechargeable AIBs. As shown in Scheme 1, an aluminium–organic battery composed of an Al metal anode, a polymer cathode, and a low-cost $AlCl_3$/urea electrolyte, illustrates the redox interactions between C=O and C=N functional groups and aluminium carrier ions during the charge/discharge process. The aluminium-organic battery renders a high discharge capacity of 295 mAh g^{-1} at the current density of 0.1 A g^{-1} and an excellent cyclability with a retention capacity of 85 mAh g^{-1} at 1 A g^{-1} after 4000 cycles. The specific energy density are 413, 291, 214, and 168 Wh kg^{-1} at different current densities, making it potentially competitive against other literature benchmarks.[5,8,19–21,25,31] The outstanding performances are closely associated with the unique nanoarchitectural design integrating redox-active C=O and C=N synergies in the conjugated polymer.[32,33] Density functional theory (DFT) studies and ex situ investigations reveal that the fused nitrogen atoms in the structure can improve the electrochemical reactivity of the polymer by assisting neighbouring carbonyl groups binding to more than one aluminium carrier ions. In addition, the rigid ladder structure and extended π-conjugation are believed to be beneficial to charge transfer performance. Further incorporation of CNTs with the polymer not only establishes a stable ionic and electronic conduction network in the cathode, but also expose the polymer with more available active sites to uptake aluminium carrier ions. This study highlights the promise of heteroatom π-conjugated polymer with multiple redox centres to realise high-performance AIBs using low-cost electrolytes.

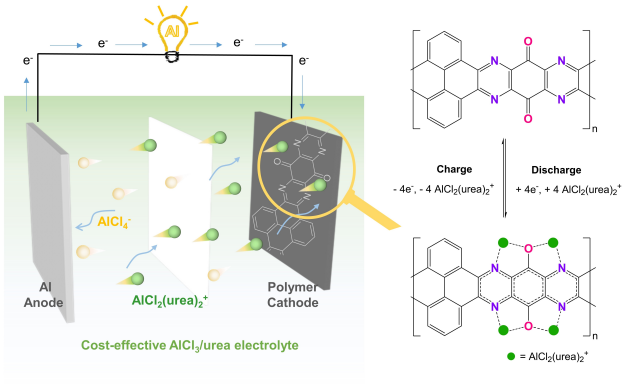

Scheme 1. Illustration of a conjugated polymer with synergistic C=O and C=N redox centres for low-cost Al–organic battery in an $AlCl_3$/urea electrolyte.

Results and Discussion

Design and Characterizations of PYTQ

The organic electrode materials with rigidly extended π-conjugation and heteroatom doping in the structure are believed to achieve good electrochemical performances. Two monomers, pyrene-4,5,9,10-tetraone (PYT) and tetraaminobenzoquinone (TABQ), were chosen to produce the aza-fused quinone polymer (PYTQ) with 1,4-pyrazine ring and carbonyl groups. The PYTQ polymer with dual redox sites (C=O and C=N) was synthesised via a simple polycondensation process according to literature with some optimizations (Supporting Information and Figures S1–S4).[34]

Fourier transform infrared (FTIR, Figure S5) spectrum of the as-synthesized PYTQ polymer resembles the vibration modes of carbonyls (C=O) and imides (C=N) groups at 1670 cm^{-1} and 1517 cm^{-1}, respectively. The peak at

1330 cm^{-1} corresponds to the aromatic C–N vibration. All these peaks reveal the successful preparation of aza-fused quinone structure. Because of the rigid structure of the π-conjugated backbone, the obtained polymer is insoluble in common deuterated nuclear magnetic resonance (NMR) solvents. The solid-state ^{13}C NMR was conducted to further verify the structure. The single-pulsed NMR spectrum clearly demonstrate four peaks (Figure S6). The peaks at around 175.41 and 142.51 ppm can be assigned to the carbonyl groups and imine groups, whereas the peaks at 127.95 and 110.16 ppm corresponds to two types of aromatic C=C bonds. By comparing solid-state cross-polarization magic angle spinning (CPMAS) solid-state ^{13}C NMR spectrum (Figure S7) and single-pulse NMR results, we can conclude that only the peak 3 at 127.95 ppm is C atom with protons in vicinity. All these results evidence the successful preparation of PYTQ polymer. According to elemental analysis (EA, Table S1), the average proportion of carbon, nitrogen, and oxygen elements accounts for 62.18, 12.53, and 22.83 wt %, respectively. With a similar C/N ratio, the average degree of polymerization was estimated to be around 10, where the molecular weight of single unit is 384 $g\,mol^{-1}$. The difference between the theoretical and experimental values can be ascribed to the residues (moisture, oxygen, etc.) encapsulated in the sample.[35]

Scanning electron microscopy (SEM, Figures S8a–c) presents the original bulky morphology of PYTQ polymer, and the microstructure can be observed from transmission electron microscopy (TEM) and high-resolution TEM (HRTEM) images (Figures S9a, b). Considering that the pristine polymer with the dense bulky structure is not favourable for fast electron transfer, PYTQ polymer-carbon nanotube (PYTQ-CNT) hybrid is therefore developed to enhance the electrical conduction channels. SEM images clearly show that CNTs interact with the PYTQ polymer, distributing and bridging the polymer into smaller sizes and better connections (Figures S8d–f). TEM images of the PYTQ-CNT hybrids further indicate the interconnection of conductive pathways between PYTQ polymer (Figures S9c, d), which will facilitate the charge transport, expose more redox centres, and render excellent stability during cycling tests. The four-probe measurements on PYTQ and PYTQ-CNT hybrids confirm an order of magnitude increase in electrical conductivity from 122 mΩ cm to $>20\times10^3$ Ω cm. Therefore, PYTQ-CNT hybrids are expected to provide a robust conductive network with increased active redox sites available to deliver high capacity in the battery tests.

Next, the X-ray photoelectron spectroscopy (XPS, Figure S10) was utilized to characterize the chemical environment in the polymer and its hybrid, where C=C, C=O, C=N and π-π interactions are displayed in both samples. The obtained samples were further characterized by powder X-ray diffraction (XRD, Figure S11). PYTQ and PYTQ-CNT show their main peak at 27.1° and 26.2° with *d* spacing of 3.3 and 3.4 Å, respectively, suggesting the π-π interactions in the conjugated polymer and hybrid.[36] Thermogravimetric analysis (TGA, Figure S12) of PYTQ polymer shows a slight weight loss before 100 °C ascribed to the solvent residues in the structure, which is consistent with the EA results. The major degradation temperature is above 400 °C, indicating an excellent thermal stability of the polymer due to its rigid ladder-like structure and strong intermolecular π-π interactions. Moreover, by integrating with CNT bridges, a broader thermal safety region can be observed for PYTQ-CNT hybrids. Adsorption–desorption isotherms (Figure S13) suggest that PYTQ-CNT hybrids possess a higher BET surface area than that of PYTQ (105.6 and 29.2 $m^2\,g^{-1}$, respectively). In addition, the pore diameter of PYTQ-CNT hybrids is featured with the mesoporous distribution. The increased surface area and pore size are important to improve affinity to electrolyte and facile diffusion of the bulky aluminium carrier ions. Thus, we expect that the PYTQ-CNT hybrids as electrodes with high surface area and good structural stability would contribute to more exposed active sites and superior electrochemical performances in AIBs

DFT Simulations

As illustrated in Scheme 1, the Al–organic battery contains an Al metal anode, a PYTQ polymer cathode, and a low-cost $AlCl_3$/urea electrolyte, where $AlCl_2(urea)_2^+$ species are responsible for energy storage according to previous studies.[27,37] In this study, DFT calculations were carried out to probe the active sites and simulate the energy storage process of PYTQ polymer accommodating $AlCl_2(urea)_2^+$ species. The isolated building block of pure PYTQ polymer is shown in Figure 1a. During the optimisation with one $AlCl_2(urea)_2^+$, the charge carrier moves toward the PYTQ polymer and places itself close to the N and O atoms. Comparing the Bader charge values of the isolated polymer and the PYTQ polymer with $AlCl_2(urea)_2^+$ (the numbers in Figures 1a, b), there are significant changes in the charge values of O and N atoms, indicating that N and O sites of the polymer are the sites that charge can accumulate. The charge distribution between the polymer and $AlCl_2(urea)_2^+$ further suggests that the prepared PYTQ polymer is conductive (Figure 1c).

To evaluate the activity of N sites of the polymer, the replacement of N by C–H in the polymer structure was performed for comparison (Figure 1d). As a result, the modified polymer without N atoms interacts less with $AlCl_2(urea)_2^+$ than the original structure, which has been well compared in terms of the atomic distances shown in Table S2. Therefore, it is reasonable to conclude that N atoms are as important as O atoms in PYTQ polymer to stabilize $AlCl_2(urea)_2^+$ in the charge transfer process. This might be attributed to the greater electronegativity of N compared to C that makes the reduction energetically more favourable. The evolution process of PYTQ polymer upon more $AlCl_2(urea)_2^+$ coordination was further simulated. DFT results suggest that having the second $AlCl_2(urea)_2^+$ on the opposite side is more favourable than having them on the same side (Figure S14 and Table S3). Accordingly, taking the advantages of synergistic C=O and C=N sites, the PYTQ polymer can accommodate up to four $AlCl_2(urea)_2^+$ per repeating unit in the energy storage process, and the optimised structures are shown in Figure 1e.[38] It is expected

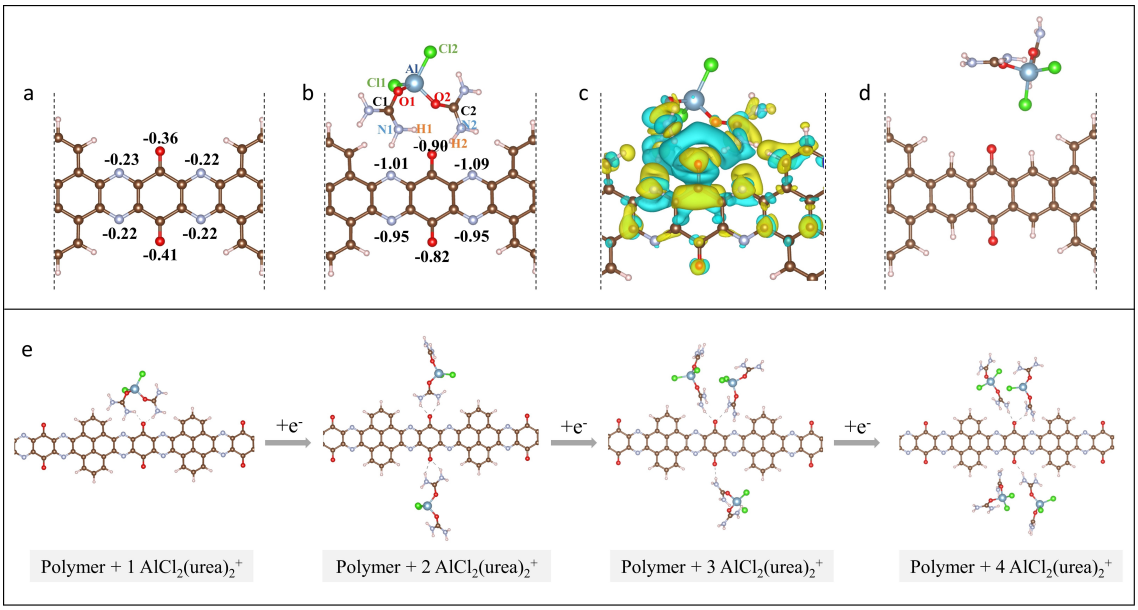

Figure 1. a) Structure of isolated building block of pure PYTQ polymer. b) The optimised structure of PYTQ polymer with one $AlCl_2(urea)_2^+$. The numbers in the structures show the calculated Bader charge values for the N and O atoms of the polymer before and after interaction with $AlCl_2(urea)_2^+$. c) Charge density difference for the optimised structure with one $AlCl_2(urea)_2^+$. d) Modified configuration when N are replaced with C–H. e) Configuration revolution of PYTQ polymer upon multi-step $AlCl_2(urea)_2^+$ accommodation. VESTA is used to produce the figures.[38]

that the heterocyclic conjugated polymer with synergistic redox sites will contribute to high aluminium uptake capacities and good stabilities in the experimental study.

Electrochemical Performances

The electrochemical properties of the PYTQ polymer were studied by using a custom-made Swagelok-type cell with the active materials as cathodes, Al foil as an anode, Mo foil as a current collector and $AlCl_3$/urea as an electrolyte (the Mo foil will not contribute any redox behaviour according to Figure S15). In the representative CV curves of PYTQ and PYTQ-CNT cathodes (Figure 2a), two obvious pairs of redox peaks at around 1.97/1.85 V and 1.60/1.36 V can be found in the initial cycle at the scan rate of 1 $mV\,s^{-1}$, indicating the reversible redox process of active sites in the prepared cathode. In the meanwhile, several flat peaks are also found, corresponding to the multi-step aluminium uptake/release processes.[39,40] The step-by-step coordination of the aluminium carrier ions with the polymer cathode is in good agreement with the DFT simulations (Figure 1e, Figure S14, Tables S2, S3). Moreover, in the PYTQ-CNT hybrid electrode, we can observe sharper redox peaks than those of PYTQ, suggesting the enhanced conductive connections between polymer and CNT.

Figure 2b shows the discharge/charge curves of the polymer cathodes at 0.2 $A\,g^{-1}$, where the discharge potentials at around 1.8 and 1.4 V agree well with CV results. PYTQ-CNT exhibits a high specific capacity of 208 $mAh\,g^{-1}$ at 0.2 $A\,g^{-1}$, while PYTQ contributes a lower specific capacity of 165 $mAh\,g^{-1}$. In contrast, CNT alone contributes a negligible specific capacity of 18 $mAh\,g^{-1}$. The rate capabilities of PYTQ-CNT and PYTQ are shown in Figure 2c. PYTQ-CNT delivers reversible capacities of 295, 208, 153, 120, and 85 $mAh\,g^{-1}$ at current densities at 0.1, 0.2, 0.5, 1, and 2 $A\,g^{-1}$, respectively. The discharge capacity then recovers to 242.4 $mAh\,g^{-1}$ when the current rate returns to 0.1 $A\,g^{-1}$, maintaining 82.2 % of the initial capacity. In the case of PYTQ, the corresponding values decrease monotonically from 208.5 to 57 $mAh\,g^{-1}$ as loading currents of increases from 0.1 to 2 $A\,g^{-1}$, which finally keeps 77.8 % of the reversible capacity at 0.1 $A\,g^{-1}$. During a long-term cycling test, PYTQ-CNT can provide a high capacity of 114 $mAh\,g^{-1}$ at 1 $A\,g^{-1}$ and retain 85 $mAh\,g^{-1}$ over 4000 cycles (Figure 2d). Increasing the current density to 2 $A\,g^{-1}$ presents 70 % capacity retention after 3500 cycles (Figure S16). While the PYTQ electrode shows capacity fading with 56 $mAh\,g^{-1}$ after 500 cycles (Figure 2d and Figure S17). Both cathodes possess high Coulombic efficiency of 100 % in the cycling test. These results reveal the incorporation of PYTQ and CNT builds up a stable ionic and electronic conduction network in the electrodes. The systematic comparison between PYTQ-CNT and other similar materials published in AIBs were listed in Table S5. Our polymer with conjugated backbone and synergistic C=O and C=N redox centres shows superior performances to the previously reported organic electrode materials with single-type of redox centre (C=O or C=N).

The energy density of electrode material is dominated by the operating voltage and specific capacity.[24] Here, considering different charge carrier ions in versatile AIBs using different electrolytes, only discharging voltage and specific capacity are accounted for the calculation and comparison (Supporting Information). The PYTQ-CNT cathode shows remarkable energy density throughout a wide

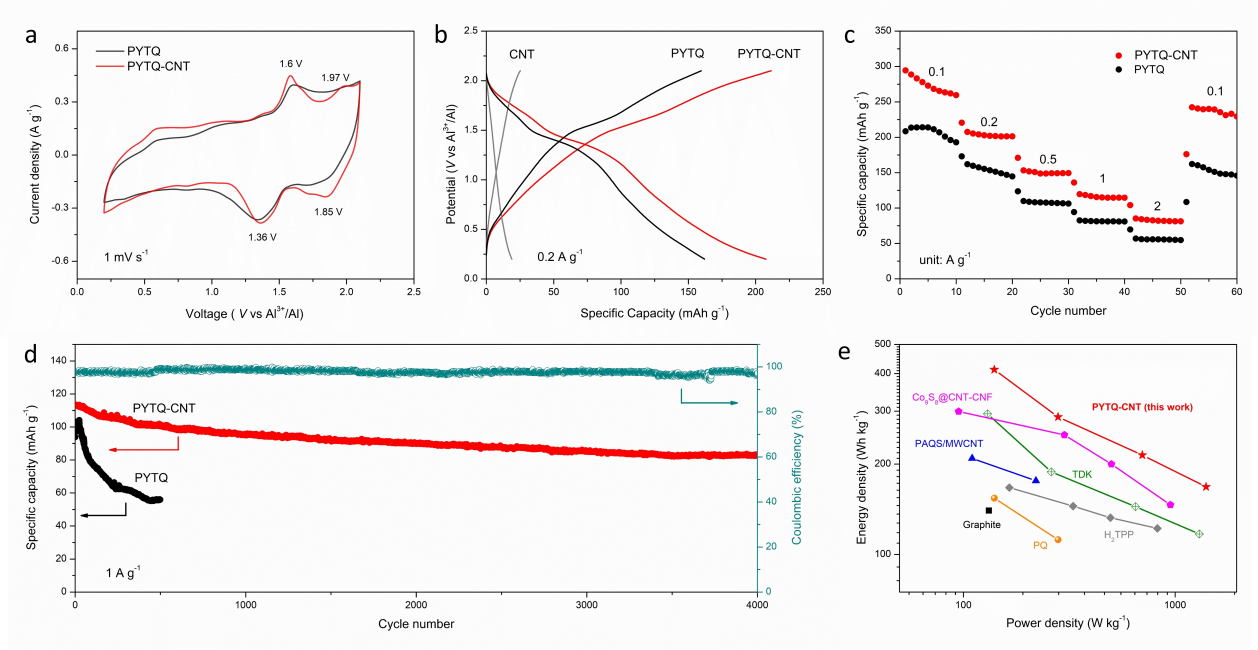

Figure 2. a) CV profiles. b) Galvanostatic discharge/charge profiles of PYTQ-CNT, PYTQ, and CNT electrodes at the current density of 0.2 A g^{-1}. c) Rate capability at different current densities. d) Cycling stability of PYTQ-CNT and PYTQ electrodes at the current density of 1 A g^{-1}. e) Ragone plots of electrode materials in AIBs.[5,8,19–21,25,31] The specific energy/power values are calculated based on the performances of cathode materials.

range of current densities (413, 291, 214, and 168 Wh kg^{-1} at 0.1, 0.2, 0.5, and 1 A g^{-1}, respectively), which are superior to most of the electrode materials in AIBs reported so far (Figure 2e).[5,8,19–21,25,31] The good battery performances of PYTQ-CNT can be attributed to the improved conductivity and sufficient electrochemically available interfaces, which facilitate fast electron and ionic transportation. The results suggest the nanoarchitectonic strategy of fused heteroaromatic building blocks to form π-conjugated polymer is highly effective for the development of high-performance AIBs.

Ex Situ Al-Storage Mechanism Analysis

To study the charging/discharging mechanism of the polymer electrode, the structure evolution was investigated via ex situ FTIR and XPS during different electrochemical reaction states with $AlCl_2(urea)_2^+$ uptake/release (Figure 3a). As shown in ex situ FTIR spectra (Figure 3b), the absorbance of C=O bands at 1670 cm^{-1} gradually disappeared during the discharging process, which corresponds to the formation of enolate for Al-storage. When the electrode is fully recharged to 2.1 V, the C=O peak recovers, representing a good reversibility of the redox interaction and release of $AlCl_2(urea)_2^+$. Another vibration absorption peak at around 1517 cm^{-1} assigned to the C=N bonds of imine groups follows similar changes in different discharged/charged states. Taken together, the results suggest both C=O and C=N groups are the active centres that have been involved in the reversible battery reactions. This is in good agreement with the DFT results that C=O and C=N are the active sites on the polymer, with which $AlCl_2(urea)_2^+$ species coordinate.

To get further insight into the reaction mechanism, ex situ XPS were measured. Figure 3c reveals the survey scan of the PYTQ electrodes. Compared with their pristine states where rare Al or Cl element is detected, the high concentration of Al and Cl signals on discharged electrodes implies the uptake of $AlCl_2(urea)_2^+$ during the discharging process. The high-resolution XPS spectra of Al 2p, Cl 2p, C 1s and N 1s are presented in Figure 3d. The subsequent charging process reduces the intensities of Al 2p and Cl 2p peaks, suggesting the release of $AlCl_2(urea)_2^+$ species. The residual sign at charged states is probably attributed to the adsorption of electrolytes. C 1s spectra reveal the changes of C–O, C=N, and C=O groups located at 286, 287 and 288.3 eV, respectively. In the discharged state, C=N and C=O bonds decrease simultaneously, whereas the C–O bond varies opposite. Once being fully recharged to 2.1 V, the intensity of the peaks presents reversible transformation. The changes of C=N sites can be further observed in the N 1s spectra. The N 1s peak of the pristine electrode at 399.6 eV stands for the C=N, while the small peak at 401.2 eV represents the C–N. For the discharged cathode, the peak for C=N decreases remarkably, accompanied by the strengthening intensity of C–N bonds. The peaks shift to lower binding energies thanks to the transformation of C=N to C–N upon the uptake of $AlCl_2(urea)_2^+$. After recharging, we may observe the recovery of the C=N bonds and the decreased intensity of C–N peaks. Also, the peaks shift back towards higher binding energies in the following charging process, indicating the redox behaviour between polymer and $AlCl_2(urea)_2^+$ is highly reversible. The peak area ratios

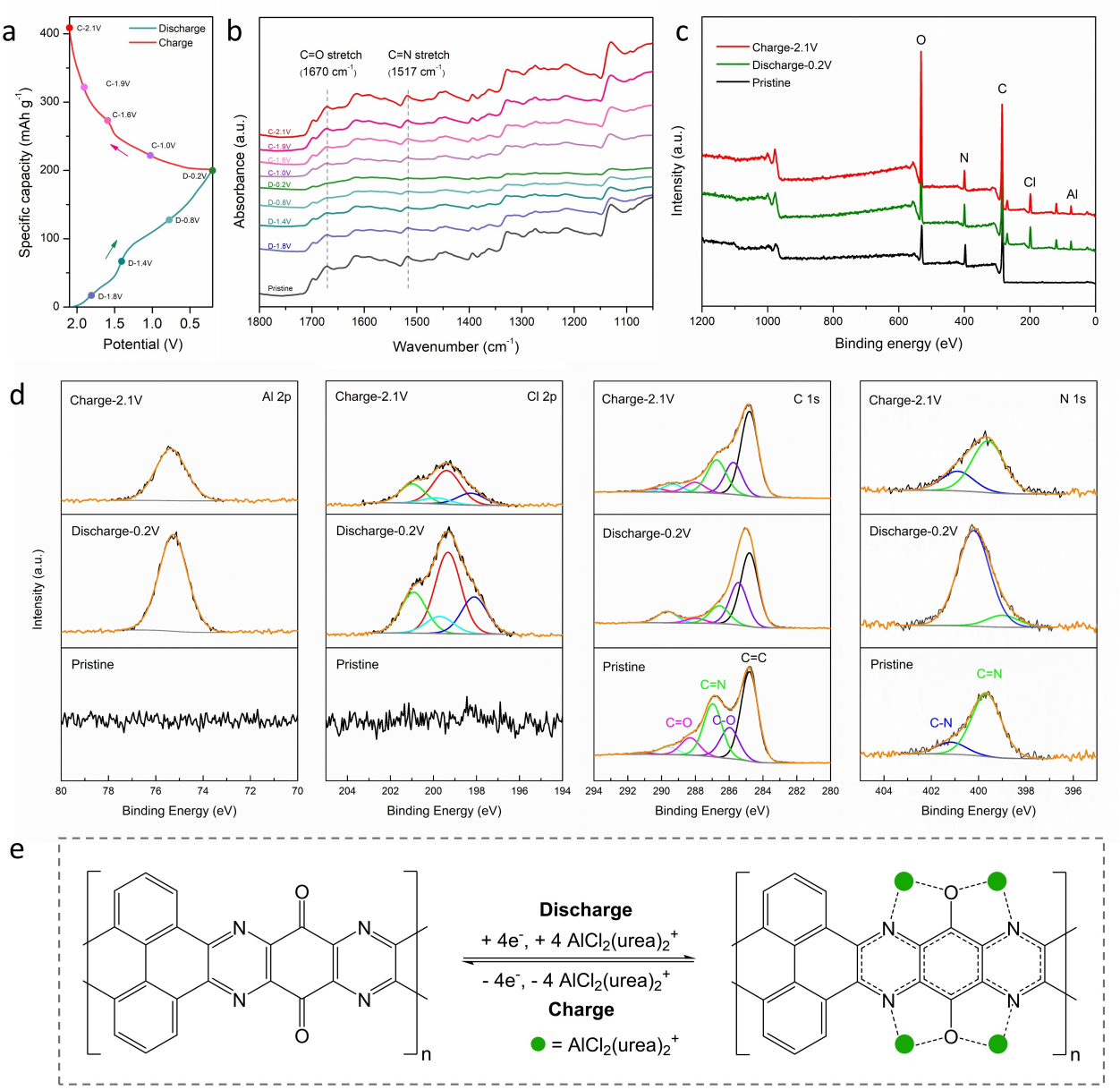

Figure 3. a) Different states in the charge-discharge curve for ex situ characterizations. b) Ex situ FTIR spectra. c) Ex situ XPS survey spectra, and d) high-resolution XPS spectra Al 2p, Cl 2p, C 1s, N 1s regions of pristine, discharged and charged states. e) The proposed redox mechanism of PYTQ polymer as cathode material in an aluminium battery with $AlCl_3$/urea electrolyte.

of these bonds provide quantitative evidence to support their changes as discussed above (Figure S18 and Table S4).

Accordingly, the C=O and C=N groups in PYTQ polymer have been experimentally confirmed as the redox active sites during the reversible charging/discharging process, which is in good agreement with the DFT simulations. The possible redox mechanism of PYTQ polymer as cathode in an aluminium battery with $AlCl_3$/urea electrolyte is shown in Figure 3e. The synergistic C=O and C=N active sites on PYTQ polymer are reduced to C–O and C–N bonds after being discharged, which further coordinate four positive $AlCl_2(urea)_2^+$ in the electrolyte, delivering a four-electron transfer per repeating unit. When the battery is recharged, the C=O and C=N sites will be recovered reversibly, therefore contributing high aluminium uptake capacities and good stabilities as suggested by DFT simulations and experimental battery performances. Ex situ analysis and theoretical DFT calculations provide deep insight into the energy storage mechanism of PYTQ polymer in AIBs.

To investigate the influence of PYTQ polymer on the anode, Al electrodes after 500 cycling test and Al foils soaked in electrolyte without cycling test were collected and analysed via SEM, XPS and Energy-Dispersive Spectroscopy (EDS), as shown in Figure S19. The Al foils after soaking in $AlCl_3$/urea electrolyte show thick artificial solid electrolyte interphases layer composed of Al oxides, Al

metals and other components consisting of C, N, Cl elements.[26] In comparison, the SEM and EDS images suggest that the polymer cathode could lead to the uniform striping/plating of Al on the anode surface after long-term cycling test, resulting in less passivated Al oxides but more active Al metals according to the XPS analysis.

Electrochemical Kinetic Analysis

Electrochemical kinetic analysis of the as-prepared electrodes was further conducted. The consecutive CV profiles were collected at scan rates of 0.2 to 1.0 mV s^{-1} (Figure 4a). There is a linear relationship between the peak current (i, A) and the sweep rate (v, mV s^{-1}) following the power-law relationship[41] as shown in Equation (1):

$$i = av^b \tag{1}$$

where i refers to the current value associated with a certain voltage, v refers to scan rate, a and b are adjustable constants. The value of b can be obtained by calculating the slope of log (v)−log (i) plots. The slope $b=0.5$ indicates a diffusion-controlled kinetic process, whereas $b=1.0$ suggests a capacitive-type behaviour. Here, the b-values calculated for peak 1 to peak 4 are 0.86, 0.91, 0.74 and 0.97, respectively (Figure 4b). The result demonstrates the fast kinetics of PYTQ-CNT electrodes in AIBs are simultaneously dominated by ionic diffusion and capacitive ion adsorption.

The mechanism from these two processes can be quantitatively described through the Equations (2), (3):[42]

$$i = k_1 v + k_2 v^{1/2} \tag{2}$$

$$iv^{1/2} = k_1 v^{1/2} + k_2 \tag{3}$$

where k_1 and k_2 are constants determined by plotting $v^{1/2}$ versus $i/v^{1/2}$ at a given potential. Thus, we further calculated the capacitive ($k_1 v$) and diffusion-controlled ($k_2 v^{1/2}$) contributions based on both k_1 and k_2. The results indicate that the capacitive contribution of the PYTQ-CNT electrode ranges from 71.7 to 84.8 % with the increase of scanning rates from 0.2 to 1.0 mV s^{-1} (Figures 4c,d). These results consequently suggest the charge storage in PYTQ-CNT appears to be both diffusion-controlled process and capacitive-limited process, enabling a high cathode capacity and fast kinetic.

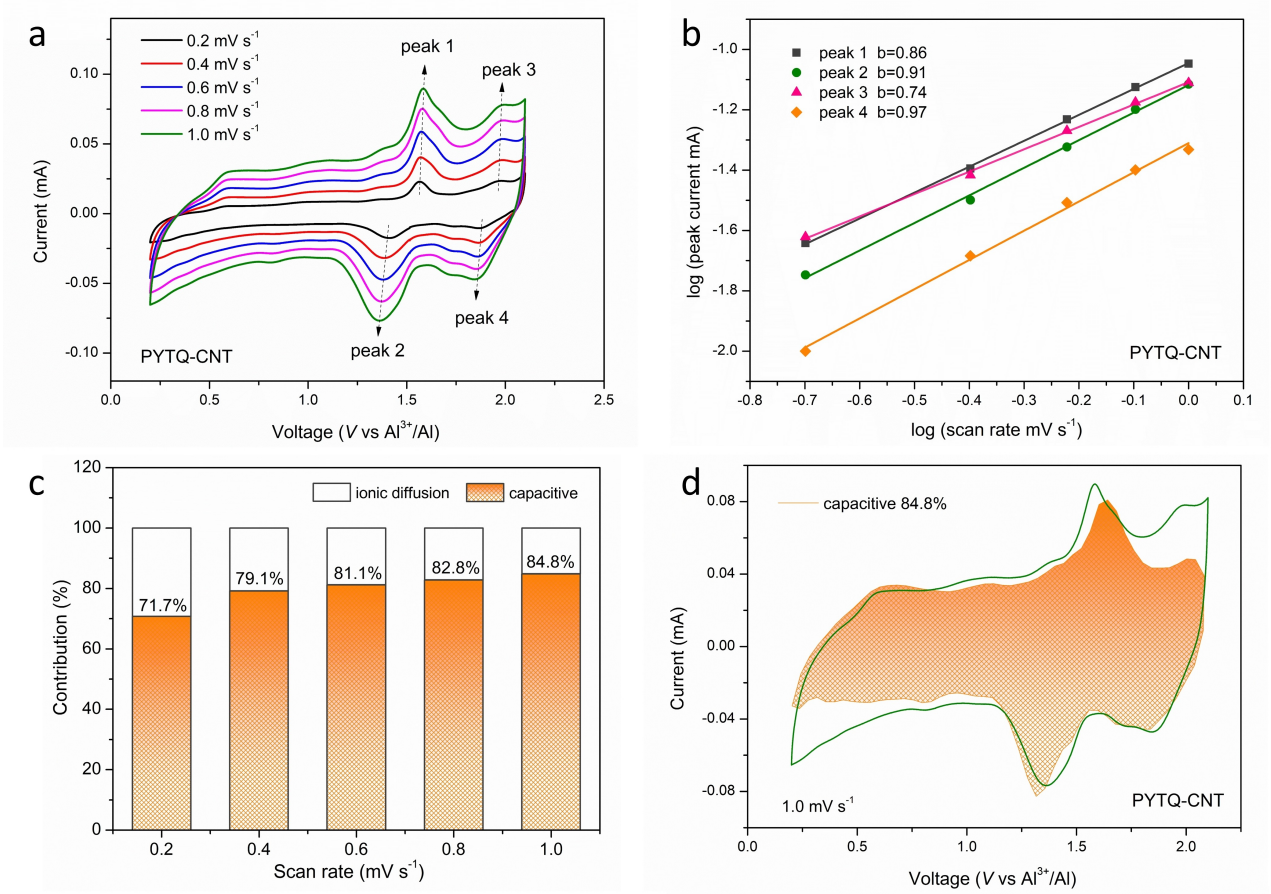

Figure 4. Electrochemical kinetic analysis of the PYTQ-CNT electrodes. a) CV profiles at different scan rates. b) The corresponding plots of log (peak current, i) vs. log (scan rate, v) and the slop b of the redox peaks. c) The capacitive contributions in PYTQ-CNT electrodes at different scan rates. d) The CV profile with the pseudocapacitive contribution of PYTQ-CNT electrodes at a scan rate of 1.0 mV s^{-1}.

To further elucidate the electrochemical kinetics of the PYTQ-CNT electrodes, electrochemical impedance spectroscopy (EIS) was performed. The Nyquist plots and equivalent circuit model for simulating the process are shown in Figure S20. The resulting fitting data suggests the charge transfer resistance and interface resistance decrease as the charge-discharge reaction proceeds, which is related to the reduced passivated oxides and the effective Al platting on the anodes. Moreover, the PYTQ-CNT electrodes exhibit smaller resistance, suggesting the good conductivity of the PYTQ-CNT hybrids that facilitate the facile charge exchange kinetics between the extended π-conjugated polymer and aluminium carrier ions.

Conclusion

In summary, we have demonstrated a heterocycle-conjugate polymer nanoarchitectural design with synergistic redox-active C=O/C=N centres and π-conjugation as a new type of organic cathode material for high-performance Al-organic batteries. Theoretical DFT and ex situ experimental studies show that the fused C=N sites in polymer not only contribute to good π-conjugation but also enhance the redox reactivity of the C=O sites, which enables the PYTQ polymer to accommodate up to four $AlCl_2(urea)_2^+$ per repeating unit in the $AlCl_3$/urea electrolyte. Benefiting from the synergistic C=O and C=N redox sites, the π-conjugated rigid structure and the conductive CNTs pathways, the polymer cathode delivers a high discharge capacity of 295 $mAh\,g^{-1}$ at 0.1 $A\,g^{-1}$, a long-term stability with a retention capacity of 85 $mAh\,g^{-1}$ at 1 $A\,g^{-1}$ after 4000 cycles, and remarkable energy densities. The electrochemical kinetic analysis reveals that the charge storage in the electrodes is dominated by both ionic diffusion and capacitive process, favouring fast $AlCl_2(urea)_2^+$ storage and pronounced long-term cyclability. The combination of redox-active heteroaromatic conjugated polymer cathode, earth-abundant Al metal anode, and low-cost $AlCl_3$/urea electrolyte should hold a great prospect for future large-scale energy storage applications.

Acknowledgements

The authors acknowledge the financial support from Australian Research Council through its Discovery, Future Fellowship, Laureate Fellowship and Linkage Programs. The authors acknowledge the access to computational resources at the NCI National Facility through the National Computational Merit Allocation Scheme supported by the Australian Government and the University of Queensland Research Computing Centre (UQ RCC). The authors also thank the scientific and technical support from the Australian Microscopy & Microanalysis Research Facility at the Centre for Microscopy and Microanalysis, the University of Queensland. Open access publishing facilitated by The University of Queensland, as part of the Wiley - The University of Queensland agreement via the Council of Australian University Librarians.

Conflict of Interest

The authors declare no conflict of interest.

Data Availability Statement

The data that support the findings of this study are available from the corresponding author upon reasonable request.

Keywords: $AlCl_3$/Urea Electrolyte · Aluminium Batteries · Heterocycles · Polymer Electrodes · Redox Chemistry

[1] T. P. Nguyen, A. D. Easley, N. Kang, S. Khan, S. M. Lim, Y. H. Rezenom, S. Wang, D. K. Tran, J. Fan, R. A. Letteri, X. He, L. Su, C. H. Yu, J. L. Lutkenhaus, K. L. Wooley, *Nature* **2021**, *593*, 61–66.
[2] J. Chen, D. H. C. Chua, P. S. Lee, *Small Methods* **2020**, *4*, 1900648.
[3] Y. Liang, H. Dong, D. Aurbach, Y. Yao, *Nat. Energy* **2020**, *5*, 646–656.
[4] S. K. Das, *Angew. Chem. Int. Ed.* **2018**, *57*, 16606–16617; *Angew. Chem.* **2018**, *130*, 16846–16857.
[5] M. C. Lin, M. Gong, B. Lu, Y. Wu, D. Y. Wang, M. Guan, M. Angell, C. Chen, J. Yang, B. J. Hwang, H. Dai, *Nature* **2015**, *520*, 324–328.
[6] T. Cai, L. Zhao, H. Hu, T. Li, X. Li, S. Guo, Y. Li, Q. Xue, W. Xing, Z. Yan, L. Wang, *Energy Environ. Sci.* **2018**, *11*, 2341–2347.
[7] H. Li, H. Yang, Z. Sun, Y. Shi, H. M. Cheng, F. Li, *Nano Energy* **2019**, *56*, 100–108.
[8] Y. Hu, D. Ye, B. Luo, H. Hu, X. Zhu, S. Wang, L. Li, S. Peng, L. Wang, *Adv. Mater.* **2018**, *30*, 1703824.
[9] G. Li, J. Tu, M. Wang, S. Jiao, *J. Mater. Chem. A* **2019**, *7*, 8368–8375.
[10] J. Tu, M. Wang, X. Xiao, H. Lei, S. Jiao, *ACS Sustainable Chem. Eng.* **2019**, *7*, 6004–6012.
[11] G. A. Elia, K. Marquardt, K. Hoeppner, S. Fantini, R. Lin, E. Knipping, W. Peters, J. F. Drillet, S. Passerini, R. Hahn, *Adv. Mater.* **2016**, *28*, 7564–7579.
[12] S. He, D. Zhang, X. Zhang, S. Liu, W. Chu, H. Yu, *Adv. Energy Mater.* **2021**, *11*, 2100769.
[13] Y. Liang, Y. Yao, *Joule* **2018**, *2*, 1690–1706.
[14] P. Poizot, J. Gaubicher, S. Renault, L. Dubois, Y. Liang, Y. Yao, *Chem. Rev.* **2020**, *120*, 6490–6557.
[15] J. Xie, Q. Zhang, *Small* **2019**, *15*, 1805061.
[16] Y. Lu, J. Chen, *Nat. Chem. Rev.* **2020**, *4*, 127–142.
[17] C. Wang, *Energy Environ. Mater.* **2020**, *3*, 441–452.
[18] K. Qin, J. Huang, K. Holguin, C. Luo, *Energy Environ. Sci.* **2020**, *13*, 3950–3992.
[19] D. J. Kim, D. J. Yoo, M. T. Otley, A. Prokofjevs, C. Pezzato, M. Owczarek, S. J. Lee, J. W. Choi, J. F. Stoddart, *Nat. Energy* **2019**, *4*, 51–59.
[20] D. J. Yoo, M. Heeney, F. Glocklhofer, J. W. Choi, *Nat. Commun.* **2021**, *12*, 2386–2394.
[21] M. Mao, C. Luo, T. P. Pollard, S. Hou, T. Gao, X. Fan, C. Cui, J. Yue, Y. Tong, G. Yang, T. Deng, M. Zhang, J. Ma, L. Suo, O. Borodin, C. Wang, *Angew. Chem. Int. Ed.* **2019**, *58*, 17820–17826; *Angew. Chem.* **2019**, *131*, 17984–17990.

[22] J. C. Chen, Q. N. Zhu, L. Jiang, R. Y. Liu, Y. Yang, M. Y. Tang, J. W. Wang, H. Wang, L. Guo, *Angew. Chem. Int. Ed.* **2021**, *60*, 5794–5799; *Angew. Chem.* **2021**, *133*, 5858–5863.
[23] J. Zhou, X. Yu, J. Zhou, B. Lu, *Energy Storage Mater.* **2020**, *31*, 58–63.
[24] F. Guo, Z. Huang, M. Wang, W. L. Song, A. Lv, X. Han, J. Tu, S. Jiao, *Energy Storage Mater.* **2020**, *33*, 250–257.
[25] J. Bitenc, N. Lindahl, A. Vizintin, M. E. Abdelhamid, R. Dominko, P. Johansson, *Energy Storage Mater.* **2020**, *24*, 379–383.
[26] Y. X. Li, L. J. Liu, Y. Lu, R. J. Shi, Y. L. Ma, Z. H. Yan, K. Zhang, J. Chen, *Adv. Funct. Mater.* **2021**, *31*, 2102063.
[27] Y. T. Kao, S. B. Patil, C. Y. An, S. K. Huang, J. C. Lin, T. S. Lee, Y. C. Lee, H. L. Chou, C. W. Chen, Y. J. Chang, Y. H. Lai, D. Y. Wang, *ACS Appl. Mater. Interfaces* **2020**, *12*, 25853–25860.
[28] C. Peng, G. H. Ning, J. Su, G. Zhong, W. Tang, B. Tian, C. Su, Di. Yu, L. Zu, J. Yang, M. F. Ng, Y. S. Hu, Y. Yang, M. Armand, K. P. Loh, *Nat. Energy* **2017**, *2*, 17074.
[29] J. Xie, P. Gu, Q. Zhang, *ACS Energy Lett.* **2017**, *2*, 1985–1996.
[30] J. Kim, J. H. Kim, K. Ariga, *Joule* **2017**, *1*, 739–768.
[31] X. Han, S. J. Li, W. L. Song, N. Chen, H. S. Chen, S. Y. Huang, S. Q. Jiao, *Adv. Energy Mater.* **2021**, *11*, 2101446.
[32] K. Ariga, Q. Ji, W. Nakanishi, J. P. Hill, M. Aono, *Mater. Horiz.* **2015**, *2*, 406–413.
[33] K. Ariga, *Nanoscale Horiz.* **2021**, *6*, 364–378.
[34] Y. Chen, H. Y. Li, M. Tang, S. M. Zhuo, Y. C. Wu, E. J. Wang, S. M. Wang, C. L. Wang, W. P. Hu, *J. Mater. Chem. A* **2019**, *7*, 20891–20898.
[35] Z. Meng, A. Aykanat, K. A. Mirica, *Chem. Mater.* **2019**, *31*, 819–825.
[36] M. Tang, S. Zhu, Z. Liu, C. Jiang, Y. Wu, H. Li, B. Wang, E. Wang, J. Ma, C. Wang, *Chem* **2018**, *4*, 2600–2614.
[37] M. Angell, C. J. Pan, Y. Rong, C. Yuan, M. C. Lin, B. J. Hwang, H. Dai, *Proc. Natl. Acad. Sci. USA* **2017**, *114*, 834–839.
[38] K. Momma, F. Izumi, *J. Appl. Crystallogr.* **2011**, *44*, 1272–1276.
[39] R. Shi, L. Liu, Y. Lu, C. Wang, Y. Li, L. Li, Z. Yan, J. Chen, *Nat. Commun.* **2020**, *11*, 178.
[40] S. Y. Yang, Y. J. Chen, G. Zhou, Z. W. Fu, *J. Electrochem. Soc.* **2018**, *165*, A1422–A1429.
[41] S. Wang, S. Huang, M. J. Yao, Y. Zhang, Z. Q. Niu, *Angew. Chem. Int. Ed.* **2020**, *59*, 11800–11807; *Angew. Chem.* **2020**, *132*, 11898–11905.
[42] W. H. Ren, Z. X. Zhu, M. S. Qin, S. Chen, X. H. Yao, Q. Li, X. M. Xu, Q. L. Wei, L. Q. Mai, C. Zhao, *Adv. Funct. Mater.* **2019**, *29*, 1806405.

Manuscript received: March 10, 2022
Accepted manuscript online: March 24, 2022
Version of record online: April 13, 2022